Structured Quantum Noise: Hyperentanglement, DOF-Resolved Dynamics and Coherence Redistribution

Deepinder Sidhu
Department of Computer Science and Electrical Engineering
University of Maryland, Baltimore County
sidhu@umbc.edu

Abstract

Quantum noise is usually represented as a completely positive trace-preserving map acting on an observed subsystem. This representation is operationally useful, but it can suppress the physical structure of the environment that generates the apparent decoherence. Independent Markovian noise primarily attenuates coherence and distinguishability. Structured environments, by contrast, may contain retained degrees of freedom, memory modes, cross-couplings, and interaction pathways capable of redistributing coherence before partially returning it to the observed subsystem.

This paper develops a degree-of-freedom-resolved framework for structured quantum noise and coherent memory dynamics and coherent memory dynamics and connects it to an exact dynamical realization motivated by hyperentangled and multi-DOF quantum systems. The central thesis is that observed decoherence need not correspond to irreversible destruction of coherence. It may instead correspond to redistribution of amplitude, phase, coherence, entanglement, and parameter sensitivity into unobserved or partially observed sectors of an enlarged Hilbert space.

The framework is realized through a minimal embedded partial-swap model involving two observed qubits and one retained memory qubit. Exact one-cycle and two-cycle coherence amplitudes are derived analytically. The observed Bell-sector coherence contains both direct survival terms and memory-mediated interference terms. The interference term produces partial coherence revival without introducing any phenomenological constructive-noise ansatz.

The reduced two-qubit density matrix is then analyzed exactly. We derive its Bell-basis diagonalization, entanglement negativity, and mixed-state Quantum Fisher Information (QFI). The same reduced coherence amplitude controls both entanglement and metrological usefulness. Finally, exact memory-retained dynamics are compared with memory-reset dynamics in numerical simulations. The simulations validate the analytic recurrence structure and demonstrate oscillatory revival of coherence and QFI due to retained pathway interference. The results provide a unified physical and mathematical account of structured quantum noise as coherence redistribution rather than scalar attenuation alone.

1 Introduction

Quantum technologies rely on the controlled preparation, transformation, and measurement of coherent quantum states. In quantum metrology, the central operational quantity is parameter distinguishability. For a phase-like parameter ϕ encoded by a generator G, an ideal pure-state family

$$|\psi_\phi\rangle = e^{-i\phi G}|\psi_0\rangle \tag{1}$$

has Quantum Fisher Information (QFI)

$$F_Q = 4\,\mathrm{Var}(G). \tag{2}$$

If coherent resources accumulate constructively, the generator variance can scale quadratically with the effective interrogation depth or resource number, yielding the familiar Heisenberg-scaling ideal [6, 9, 10].

Real systems are not isolated. Environmental coupling, dephasing, amplitude damping, photon loss, motional noise, and imperfect control reduce distinguishability and suppress useful quantum correlations. In the standard reduced-channel view, the observed state evolves according to

$$\rho_S \longmapsto \mathcal{E}(\rho_S), \tag{3}$$

where $\mathcal{E}$ is a completely positive trace-preserving (CPTP) map [5,8,15]. For independent Markovian decoherence, this channel description is often accurately summarized at the architecture level by an attenuation envelope. For example, a noise-limited effective QFI may be written as

$$F_Q^{\text{eff}}(L) = L^2\Lambda(L), \tag{4}$$

where L is a coherent interrogation depth and $\Lambda(L)$ is a coherence-retention factor. If

$$\Lambda(L) = e^{-\gamma L}, \tag{5}$$

then

$$F_Q^{\text{eff}}(L) = L^2 e^{-\gamma L}. \tag{6}$$

The nonzero optimum occurs at

$$L^* = \frac{2}{\gamma}. \tag{7}$$

This standard result expresses the destructive-noise tradeoff: increasing coherent depth improves ideal sensitivity, but also increases exposure to decoherence.

The present paper starts from the observation that this scalar-attenuation view is not the full physical story. Microscopically, the combined system and environment evolve unitarily:

$$\rho_{SE}(t) = U(t)\rho_{SE}(0)U^\dagger(t), \tag{8}$$

while the observed state is obtained by tracing out unobserved degrees of freedom:

$$\rho_S(t) = \mathrm{Tr}_E[\rho_{SE}(t)]. \tag{9}$$

Thus, what appears as decoherence in the reduced subsystem may correspond to redistribution of amplitude, phase, coherence, and entanglement into a larger Hilbert space. If the environment rapidly disperses this information, the reduced dynamics appears Markovian. If the environment retains correlations and later re-couples to the subsystem, the lost coherence may partially return.

This distinction is particularly relevant for hyperentangled and multi-degree-of-freedom (multi-DOF) systems. Hyperentanglement distributes quantum information across more than one physical degree of freedom, such as polarization and path in photonic systems [1–3, 7, 14]. If noise acts selectively on one DOF or one path, another DOF may retain useful correlations. If the environment itself also has memory or internal structure, coherence can move through a network of system and environment pathways before returning to the observed sector.

The goal of this paper is to turn that physical intuition into a precise framework and an exact minimal realization. The paper makes four contributions.

First, it develops a DOF-resolved interpretation of structured quantum noise. In this framework, noise is not classified only by strength. It is classified by which system DOFs couple to which environmental DOFs, whether pathways are retained or reset, and how amplitudes interfere when they return.

Second, it introduces a minimal embedded partial-swap model involving two observed qubits and one retained memory qubit. This model is exactly unitary on the full three-qubit Hilbert space and becomes noisy only after the memory qubit is traced out.

Third, it derives the reduced Bell-sector coherence analytically. After one cycle, coherence is attenuated. After two cycles, a memory-mediated interference term appears and produces partial revival.

Fourth, it derives the exact entanglement negativity and mixed-state QFI of the reduced two-qubit state. The same reduced coherence amplitude controls both quantities. Numerical simulations then compare retained-memory dynamics with memory-reset dynamics, demonstrating oscillatory coherence and QFI revival.

The paper does not claim that all noise is beneficial, nor that all non-Markovianity improves performance. The present model is intentionally coherent, finite-dimensional, and globally unitary. The present model is intentionally coherent, finite-dimensional, and globally unitary. The claim is narrower and exact: retained interaction pathways can redistribute and later return coherence and parameter sensitivity through memory-mediated interference.

2 DOF-Resolved Structured Quantum Noise

2.1 Structured system and environment Hilbert spaces

Let the observed subsystem have several controllable degrees of freedom:

$$\mathcal{H}_S = \bigotimes_{\alpha=1}^{m} \mathcal{H}_S^{(\alpha)}, \tag{10}$$

where α may denote polarization, path, spin, orbital state, time-bin, frequency, motional state, or another experimentally accessible DOF. Likewise, let the environment decompose as

$$\mathcal{H}_E = \bigotimes_{\mu=1}^{M} \mathcal{H}_E^{(\mu)}. \tag{11}$$

The full Hilbert space is therefore

$$\mathcal{H}_{SE} = \left(\bigotimes_{\alpha=1}^{m} \mathcal{H}_S^{(\alpha)}\right) \otimes \left(\bigotimes_{\mu=1}^{M} \mathcal{H}_E^{(\mu)}\right). \tag{12}$$

A Hamiltonian compatible with this structure can contain system-local, environment-local, and interaction terms:

$$H = H_S + H_E + H_{SE}, \tag{13}$$

where schematically

$$H_S = \sum_{\alpha} H_S^{(\alpha)} + \sum_{\alpha<\beta} H_S^{(\alpha\beta)} + \cdots, \tag{14}$$

$$H_E = \sum_{\mu} H_E^{(\mu)} + \sum_{\mu<\nu} H_E^{(\mu\nu)} + \cdots, \tag{15}$$

and

$$H_{SE} = \sum_{\alpha,\mu} H_{S^{(\alpha)}E^{(\mu)}} + \sum_{\alpha,\beta,\mu} H_{S^{(\alpha)}S^{(\beta)}E^{(\mu)}} + \sum_{\alpha,\mu,\nu} H_{S^{(\alpha)}E^{(\mu)}E^{(\nu)}} + \cdots . \tag{16}$$

The first interaction class represents DOF-selective noise. The second and third classes represent cross-DOF and memory-bearing interactions. Such terms are precisely what scalar attenuation models suppress.

2.2 Coherence redistribution

For a selected observed coherence functional $C_S(t)$, one should not assume as a fundamental principle that

$$C_S(t) = C_S(0)e^{-\gamma t}. \tag{17}$$

That form is an effective model for particular Markovian limits. In a structured environment, the full unitary dynamics may redistribute coherence among observed DOFs, environmental DOFs, and system–environment correlations:

$$C_{\text{total}} \sim C_S(t) + C_E(t) + C_{SE}(t) + C_{\text{cross}}(t). \tag{18}$$

This equation is a bookkeeping statement, not a universal conservation law for an arbitrary coherence monotone. Its purpose is to emphasize that reduced-system loss need not imply global destruction.

In this view, decoherence is a reduced shadow of larger Hilbert-space dynamics. If the environment retains relevant correlations, then a later increase in reduced-system coherence, distinguishability, or QFI is not mysterious. It indicates that some parameter-relevant information temporarily stored outside the observed subsystem has returned.

2.3 DOF interaction pathways

A DOF interaction pathway is an ordered sequence of interaction operators,

$$\mathcal{P} = (H_{i_1j_1}, H_{i_2j_2}, \ldots, H_{i_rj_r}), \tag{19}$$

that transfers amplitude, phase, coherence, or entanglement among selected system and environment DOFs. Examples include

$$S^{(\alpha)} \to E^{(\mu)} \to S^{(\beta)} \tag{20}$$

and, in the minimal model developed below,

$$AB \to AN \to BN \to AB. \tag{21}$$

The observed coherence is generally a coherent sum over pathways. If the pathways are retained, the amplitudes may interfere. If the pathways are erased or reset, the interference terms disappear. This is the structural difference between memory-retained and memory-reset dynamics.

2.4 Hyperentanglement as motivation

Hyperentanglement provides a natural physical setting for this framework. A hyperentangled photonic state may involve simultaneous entanglement in polarization and path:

$$\mathcal{H}_S = \mathcal{H}_{\text{pol}} \otimes \mathcal{H}_{\text{path}}, \tag{22}$$

with representative structure

$$|\Psi\rangle_{\mathrm{HE}} = |\Psi\rangle_{\mathrm{pol}} \otimes |\Psi\rangle_{\mathrm{path}}. \tag{23}$$

More generally, physical systems may combine spin, path, frequency, time-bin, motional, cavity, valley, charge, or orbital sectors. Hyperentanglement is important here not because the minimal model below exhausts all hyperentangled dynamics, but because it motivates the core modeling question: where is coherence stored, through which DOF pathways does it move, and when can it return?

Prior work on hyperentanglement has emphasized enhanced communication capacity, purification, robust correlations, and illumination-related advantages [3, 11, 13, 14]. The present paper asks a complementary dynamical question: how should noise itself be modeled when both system and environment possess structured DOFs?

Existing non-Markovian studies often characterize information backflow through distinguishability measures or master-equation properties [4, 12]. The present work instead derives explicit coherence and QFI recurrence directly from exact embedded interaction pathways.

3 Exact Embedded Partial-Swap Dynamics

3.1 Three-qubit memory model

Consider two observed qubits A and B and one memory qubit N. The basis ordering is

$$|A\,B\,N\rangle. \tag{24}$$

The initial state is

$$|\Psi_0\rangle = \frac{1}{\sqrt{2}}\left(|000\rangle + |110\rangle\right). \tag{25}$$

The observed pair AB begins in a Bell-correlated sector, while N begins in $|0\rangle$.

Define the embedded swap operators

$$S_{AN}^{(3)}|a\,b\,n\rangle = |n\,b\,a\rangle, \qquad S_{BN}^{(3)}|a\,b\,n\rangle = |a\,n\,b\rangle. \tag{26}$$

The corresponding partial-swap unitaries are

$$U_{AN}(\theta) = \cos\theta\, I_8 - i\sin\theta\, S_{AN}^{(3)}, \tag{27}$$

$$U_{BN}(\theta) = \cos\theta\, I_8 - i\sin\theta\, S_{BN}^{(3)}. \tag{28}$$

A full cycle is

$$W(\theta) = U_{BN}(\theta)U_{AN}(\theta). \tag{29}$$

After r cycles,

$$|\Psi_{2r}\rangle = W(\theta)^r|\Psi_0\rangle. \tag{30}$$

The reduced state of the observed pair is

$$\rho_{AB}^{(2r)} = \mathrm{Tr}_N\left(|\Psi_{2r}\rangle\langle\Psi_{2r}|\right). \tag{31}$$

We track the Bell-sector coherence

$$c_r = \left(\rho_{AB}^{(2r)}\right)_{00,11}. \tag{32}$$

3.2 One-cycle attenuation

Applying U_{AN} to Eq. (25),

$$|\Psi_1\rangle = \frac{1}{\sqrt{2}} \left(e^{-i\theta}|000\rangle + \cos\theta|110\rangle - i\sin\theta|011\rangle \right). \tag{33}$$

Applying U_{BN},

$$|\Psi_2\rangle = \frac{1}{\sqrt{2}} \left(e^{-i2\theta}|000\rangle + \cos^2\theta|110\rangle - i\cos\theta\sin\theta|101\rangle - ie^{-i\theta}\sin\theta|011\rangle \right). \tag{34}$$

When tracing out N, only terms with the same memory state contribute to the reduced coherence between $|00\rangle$ and $|11\rangle$. The relevant terms $|000\rangle$ and $|110\rangle$ both have $N = 0$. Therefore,

$$c_1 = \left(\rho_{AB}^{(2)}\right)_{00,11} = \frac{1}{2}\cos^2\theta\, e^{-i2\theta}. \tag{35}$$

The phase factor represents coherent phase evolution; the factor $\cos^2\theta$ is attenuation due to amplitude redistribution into memory-containing sectors.

3.3 Two-cycle interference and revival

After a second cycle,

$$|\Psi_4\rangle = W(\theta)^2|\Psi_0\rangle. \tag{36}$$

The Bell-sector coherence is

$$c_2 = \left(\rho_{AB}^{(4)}\right)_{00,11} = \frac{1}{2}\left(\cos^4\theta\, e^{-i4\theta} - 2\cos\theta\sin^2\theta\, e^{-i3\theta}\right). \tag{37}$$

The first term is the direct survival path. The second term is memory-mediated interference. It arises from amplitude that leaves the original Bell sector, enters sectors involving the memory qubit, and later re-enters the observed Bell-sector matrix element.

For $\theta = \pi/4$,

$$|c_1| = \frac{1}{4}, \qquad |c_2| = \frac{\sqrt{5}}{8} \approx 0.2795. \tag{38}$$

Thus,

$$|c_2| > |c_1|. \tag{39}$$

The observed Bell-sector coherence partially revives. This revival is not imposed by a phenomenological ansatz; it follows from exact unitary dynamics and partial tracing.

3.4 General pathway expansion

For multiple cycles,

$$c_r = \left(\rho_{AB}^{(2r)}\right)_{00,11} = \frac{1}{2}\sum_k A_{r,k}(\theta)e^{-ik\theta}, \tag{40}$$

where $A_{r,k}(\theta)$ are polynomials in $\cos\theta$ and $\sin\theta$. This expression makes the pathway structure explicit. Each phase factor represents a distinct accumulated phase history, while each coefficient encodes the amplitude weight of a family of swap-mediated paths.

The recurrence is therefore an interference spectrum. Markovian reset removes cross-cycle phase memory. Retained memory preserves the pathway phases and allows revivals.

4 Reduced-State Coherence, Negativity, and QFI

4.1 Reduced Bell-sector state

The reduced two-qubit Bell-sector state is

$$\rho(c) = \frac{1}{2}|00\rangle\langle 00| + \frac{1}{2}|11\rangle\langle 11| + \frac{c}{2}|00\rangle\langle 11| + \frac{c}{2}|11\rangle\langle 00|. \tag{41}$$

In the computational basis $\{|00\rangle, |01\rangle, |10\rangle, |11\rangle\}$,

$$\rho(c) = \begin{pmatrix} 1/2 & 0 & 0 & c/2 \\ 0 & 0 & 0 & 0 \\ 0 & 0 & 0 & 0 \\ c/2 & 0 & 0 & 1/2 \end{pmatrix}. \tag{42}$$

In the exact partial-swap model, $c = c_r$ at cycle r.

4.2 Bell-basis diagonalization

Define

$$|\Phi^+\rangle = \frac{|00\rangle + |11\rangle}{\sqrt{2}}, \qquad |\Phi^-\rangle = \frac{|00\rangle - |11\rangle}{\sqrt{2}}. \tag{43}$$

Then

$$\rho(c)|\Phi^+\rangle = \frac{1+c}{2}|\Phi^+\rangle, \qquad \rho(c)|\Phi^-\rangle = \frac{1-c}{2}|\Phi^-\rangle. \tag{44}$$

The nonzero eigenvalues are

$$\lambda_+ = \frac{1+c}{2}, \qquad \lambda_- = \frac{1-c}{2}. \tag{45}$$

4.3 Exact QFI

Let the parameter be encoded by the collective generator

$$J_z = \frac{1}{2}\left(\sigma_z^{(1)} + \sigma_z^{(2)}\right). \tag{46}$$

Using

$$J_z|00\rangle = |00\rangle, \qquad J_z|11\rangle = -|11\rangle, \tag{47}$$

we obtain

$$J_z|\Phi^+\rangle = |\Phi^-\rangle, \qquad J_z|\Phi^-\rangle = |\Phi^+\rangle. \tag{48}$$

For a mixed state with spectral decomposition $\rho = \sum_a \lambda_a |a\rangle\langle a|$, the generator-form QFI is

$$F_Q(\rho, G) = 2\sum_{a,b} \frac{(\lambda_a - \lambda_b)^2}{\lambda_a + \lambda_b} |\langle a|G|b\rangle|^2, \tag{49}$$

where terms with $\lambda_a + \lambda_b = 0$ are omitted [9, 10].

Only the ordered pairs $(+,-)$ and $(-,+)$ contribute. Since

$$\lambda_+ - \lambda_- = c, \qquad \lambda_+ + \lambda_- = 1, \tag{50}$$

and

$$|\langle\Phi^+|J_z|\Phi^-\rangle|^2 = |\langle\Phi^-|J_z|\Phi^+\rangle|^2 = 1, \tag{51}$$

we obtain

$$F_Q(\rho(c), J_z) = 2c^2 + 2c^2 = 4c^2. \tag{52}$$

For coherent interrogation depth L, the generator becomes LJ_z, giving

$$F_Q(\rho(c), LJ_z) = 4L^2c^2. \tag{53}$$

In the exact partial-swap model, the cycle number r indexes repeated applications of the memory-mediated interaction. In the simulations below, the coherent interrogation depth is identified with the cycle number, $L \equiv r$. Thus,

$$F_Q^{(r)} = 4r^2|c_r|^2. \tag{54}$$

4.4 Negativity

The partial transpose with respect to subsystem B maps

$$|ij\rangle\langle kl| \mapsto |il\rangle\langle kj|. \tag{55}$$

Applying this operation to Eq. (41) gives

$$\rho^{T_B}(c) = \begin{pmatrix} 1/2 & 0 & 0 & 0 \\ 0 & 0 & c/2 & 0 \\ 0 & c/2 & 0 & 0 \\ 0 & 0 & 0 & 1/2 \end{pmatrix}. \tag{56}$$

The eigenvalues are

$$\left\{ \frac{1}{2}, \frac{1}{2}, \frac{c}{2}, -\frac{c}{2} \right\}. \tag{57}$$

Therefore, the negativity is

$$\mathcal{N}(\rho(c)) = \frac{|c|}{2}. \tag{58}$$

Equations (52) and (58) show that the same reduced coherence amplitude controls both metrological usefulness and entanglement.

5 Simulation Results and Discussion

5.1 Numerical implementation

The exact dynamics were implemented using the embedded 8×8 matrices $S_{AN}^{(3)}$ and $S_{BN}^{(3)}$ from Eq. (26). For each value of θ and cycle number r, the code computed

$$|\Psi_{2r}\rangle = W(\theta)^r |\Psi_0\rangle \tag{59}$$

and then constructed

$$\rho_{AB}^{(2r)} = \mathrm{Tr}_N \left(|\Psi_{2r}\rangle\langle\Psi_{2r}| \right). \tag{60}$$

The Bell-sector coherence c_r was extracted from Eq. (32), and the reduced-state QFI was computed using the spectral expression in Eq. (49). The derivative of $W(\theta)^r$ with respect to θ was evaluated by the exact product rule,

$$\frac{\partial W^r}{\partial \theta} = \sum_{m=0}^{r-1} W^m \frac{\partial W}{\partial \theta} W^{r-1-m}. \tag{61}$$

The implementation was checked in three ways. First, $W^\dagger W = I$ was verified to numerical precision. Second, the numerical one-cycle coherence matched Eq. (35). Third, the numerical two-cycle coherence matched Eq. (37). These checks confirm that the simulation implements the same embedded partial-swap model derived analytically.

5.2 Memory-retained versus memory-reset dynamics

The retained-memory evolution uses the same memory qubit N throughout:

$$|\Psi_{2r}\rangle = W(\theta)^r|\Psi_0\rangle. \tag{62}$$

A memory-reset reference is obtained by tracing out N after each cycle and resetting it to $|0\rangle_N$ before the next cycle. This removes cross-cycle pathway memory while preserving the same local cycle interaction.

This comparison is important because it avoids introducing any phenomenological attenuation baseline. Both curves arise from explicit dynamics. The difference is whether the environment retains memory between cycles.

5.3 Coherence revival

Figure 1 compares the Bell-sector coherence for retained-memory and memory-reset dynamics. The retained-memory curve exhibits oscillatory revivals, reflecting interference among pathways that remain phase coherent across cycles.

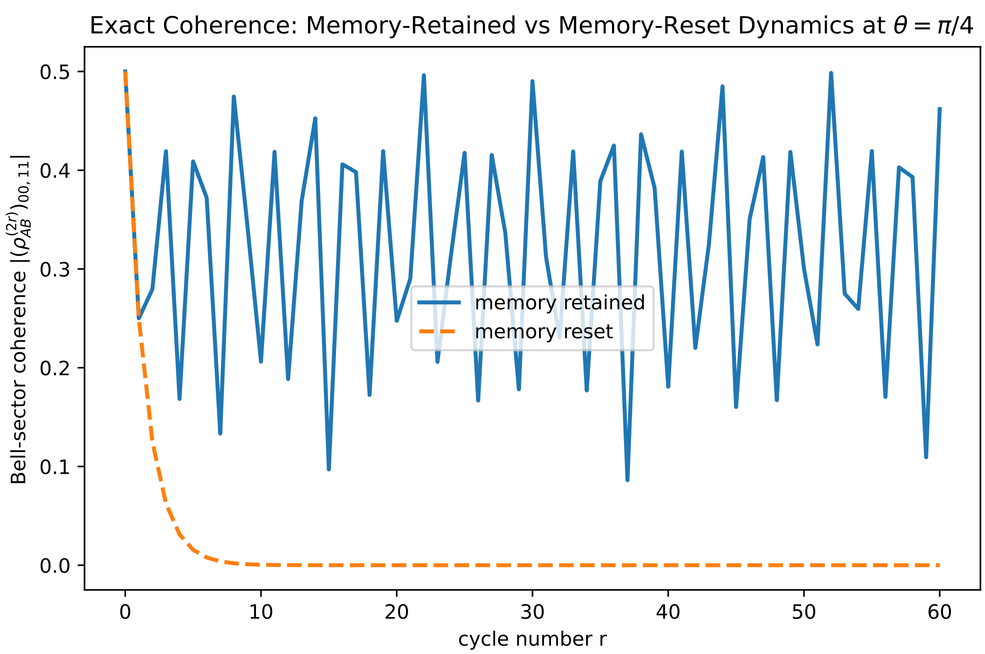

Figure 1: Bell-sector coherence under memory-retained and memory-reset dynamics. Retained memory preserves pathway interference and permits oscillatory coherence revival. Resetting the memory suppresses recurrent pathway structure.

5.4 QFI revival

Figure 2 compares exact reduced-state QFI under the same two dynamics. Since the QFI is controlled by the reduced coherence amplitude, memory-mediated coherence return produces corresponding revival in parameter sensitivity.

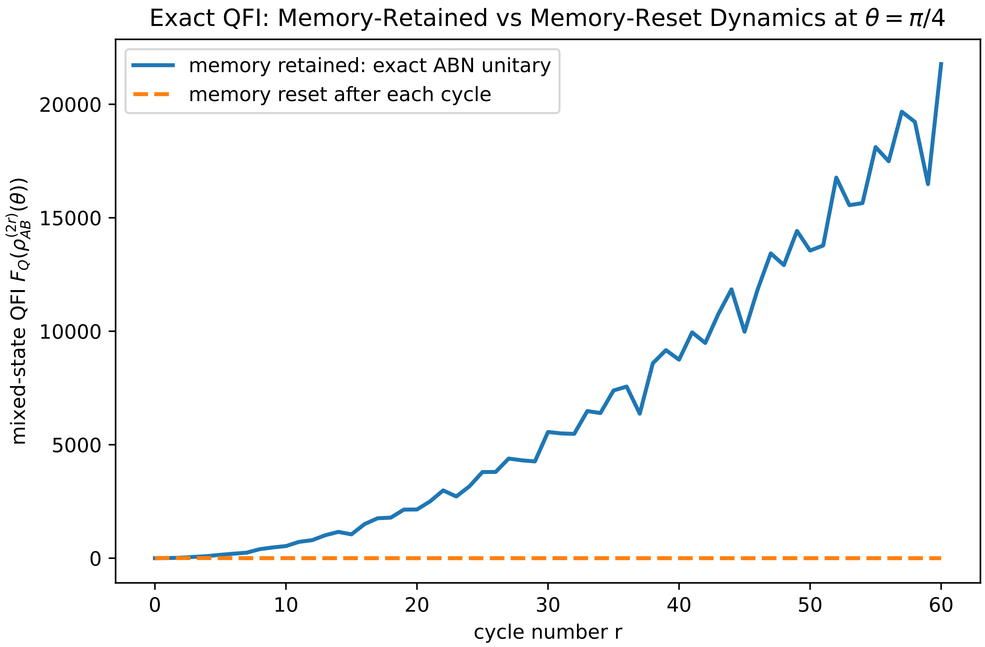

Figure 2: Exact reduced-state QFI under memory-retained and memory-reset dynamics. Retained-memory evolution exhibits oscillatory recovery of parameter sensitivity due to coherence return from retained pathways.

Because the retained-memory environment is finite-dimensional and globally unitary, the reduced-state QFI is not subject to irreversible asymptotic exponential suppression in the present model. Continued growth over the plotted range should therefore be interpreted as coherent-depth amplification sustained by recurrent memory-mediated coherence, not as a claim that arbitrary dissipative noise improves indefinitely.

Figure 3 shows the same effect in the metrological language of coherent interrogation depth. The retained-memory curve is compared against both the memory-reset dynamics and an attenuation-only reference. This figure emphasizes that the retained-memory model is a coherent finite-dimensional memory model rather than an irreversible dissipative bath.

Missing file: fig4_qfi_vs_L_exact_memory.pdf

Figure 3: Effective QFI versus coherent interrogation depth L for exact memory-retained dynamics, memory-reset dynamics, and an attenuation-only reference. In the retained-memory model, recurrent coherence can sustain QFI growth over the plotted range because the environment is coherent, finite-dimensional, and globally unitary.

Figure 4 shows the dependence of the exact retained-memory QFI on both cycle number and partial-swap angle. The revival structure is not a single-point artifact at $\theta = \pi/4$; the period, amplitude, and metrological usefulness of the recurrence depend strongly on the eigenphase structure of $W(\theta)$.

Missing file: fig5_qfi_theta_dependence_heatmap.pdf

Figure 4: Exact QFI dependence on cycle number L and partial-swap angle θ. The revival structure is strongly θ-dependent, reflecting the eigenphase spectrum of the exact cycle operator $W(\theta)$.

The memory-mediated QFI excess may still be defined as

$$\Delta F_Q(r) = F_Q^{\mathrm{mem}}(r) - F_Q^{\mathrm{reset}}(r). \tag{63}$$

Positive intervals $\Delta F_Q(r) > 0$ identify regimes where retained pathway interference improves accessible parameter sensitivity relative to reset dynamics.

5.5 Interpretation

At $\theta = \pi/4$, the coherence revivals exhibit a near-periodic spacing of roughly three cycles. This spacing is not imposed externally; it arises from eigenphase differences of the exact cycle operator $W(\theta)$. The recurrence pattern is therefore a finite-dimensional beating phenomenon among retained memory-mediated pathways. Changing θ changes the eigenphase spectrum and therefore changes the revival period, amplitude, and QFI response.

The simulations confirm the analytic mechanism. Revival is not caused by an inserted constructive-noise term. It arises because the environment retains phase-carrying pathways that later interfere in the observed Bell sector.

This gives a precise operational meaning to constructive structured noise in the present setting:

$$\text{constructive structured noise} \quad \Longleftrightarrow \quad F_Q^{\mathrm{mem}}(r) > F_Q^{\mathrm{reset}}(r). \tag{64}$$

The comparison is not between the exact model and an arbitrary decay curve. It is between two explicit dynamics differing only in whether memory is retained or erased.

The result also clarifies the role of hyperentanglement and multi-DOF architectures. Such systems naturally contain multiple storage and routing sectors. Whether noise is destructive or partially recoverable depends not only on the coupling strength, but on the pathway topology and memory retention structure.

The present model is intentionally coherent, finite-dimensional, and non-dissipative at the global level. Consequently, the observed reduced-state decoherence does not arise from irreversible thermal dissipation into an infinite bath. Instead, coherence is redistributed into retained memory pathways and later partially returned through interference among exact interaction histories. The resulting QFI revival therefore reflects structured coherent memory dynamics rather than conventional Markovian attenuation.

Accordingly, the present results should not be interpreted as a universal constructive-noise theorem. Rather, they provide an exact proof-of-mechanism demonstrating how retained interaction pathways can produce reduced-state coherence and QFI revival.

6 Conclusion

This paper developed a DOF-resolved framework for structured quantum noise and connected it to exact memory-mediated recurrence dynamics motivated by hyperentangled and multi-DOF systems.

The main result is that observed decoherence can correspond to redistribution rather than irreversible destruction of coherence. In the embedded partial-swap model, Bell-sector coherence attenuates after one cycle, but a memory-mediated interference term appears after two cycles and produces partial revival. This revival follows from exact unitary dynamics and partial tracing over a retained memory qubit.

The reduced-state analysis established that the same coherence amplitude controls entanglement negativity and Quantum Fisher Information:

$$\mathcal{N}(\rho(c)) = \frac{|c|}{2}, \qquad F_Q(\rho(c), J_z) = 4c^2. \tag{65}$$

Thus, memory-mediated coherence return can also produce QFI revival.

The simulations validate the analytic recurrence structure and compare memory-retained dynamics with memory-reset dynamics. Positive QFI excess identifies intervals where retained memory pathways increase accessible parameter sensitivity relative to reset evolution.

The broader conclusion is that quantum noise should not be classified only by strength. It must also be classified by structure: DOF connectivity, pathway geometry, memory retention, and interference topology. Independent Markovian noise primarily attenuates observable coherence. Structured environments with retained pathways can redistribute, store, and return coherence and parameter sensitivity.

This does not imply that all noise is beneficial. It shows something narrower and more precise: retained interaction pathways can produce coherence and QFI revival through memory-mediated interference. Future work should extend the analysis to higher-dimensional environments, many-body structured reservoirs, hyperentangled sensing platforms, collision models, and experimentally realizable memory-engineered metrology systems. Noise is therefore not merely attenuation; it is structured dynamics in an enlarged Hilbert space.

References

[1] Marco Barbieri, Concita Cinelli, Paolo Mataloni, and Francesco De Martini. Polarization-momentum hyperentangled states: Realization and characterization. *Physical Review A*, 72:052110, 2005.

[2] Julio T. Barreiro, Nathan K. Langford, Nicholas A. Peters, and Paul G. Kwiat. Generation of hyperentangled photon pairs. *Physical Review Letters*, 95:260501, 2005.

[3] Julio T. Barreiro, Tzu-Chieh Wei, and Paul G. Kwiat. Beating the channel capacity limit for linear photonic superdense coding. *Nature Physics*, 4:282–286, 2008.

[4] Heinz-Peter Breuer, Elsi-Mari Laine, and Jyrki Piilo. Measure for the degree of non-markovian behavior of quantum processes. *Physical Review Letters*, 103:210401, 2009.

[5] Heinz-Peter Breuer and Francesco Petruccione. *The Theory of Open Quantum Systems*. Oxford University Press, 2002.

[6] Vittorio Giovannetti, Seth Lloyd, and Lorenzo Maccone. Quantum metrology. *Physical Review Letters*, 96:010401, 2006.

[7] Paul G. Kwiat. Hyper-entangled states. *Journal of Modern Optics*, 44:2173–2184, 1997.

[8] Michael A. Nielsen and Isaac L. Chuang. *Quantum Computation and Quantum Information.* Cambridge University Press, 2010.

[9] Matteo G. A. Paris. Quantum estimation for quantum technology. *International Journal of Quantum Information*, 7:125–137, 2009.

[10] Luca Pezzè, Augusto Smerzi, Markus K. Oberthaler, Roman Schmied, and Philipp Treutlein. Quantum metrology with nonclassical states of atomic ensembles. *Reviews of Modern Physics*, 90:035005, 2018.

[11] A. V. Prabhu, B. Suri, and C. M. Chandrashekar. Hyperentanglement-enhanced quantum illumination. *Physical Review A*, 103:052608, 2021.

[12] Angel Rivas, Susana F. Huelga, and Martin B. Plenio. Quantum non-markovianity: Characterization, quantification and detection. *Reports on Progress in Physics*, 77:094001, 2014.

[13] Akshay Kannan Sairam and C. M. Chandrashekar. Noise resilience in path-polarization hyperentangled probe states. *arXiv preprint arXiv:2205.13288*, 2022.

[14] Christoph Simon and Jian-Wei Pan. Polarization entanglement purification using spatial entanglement. *Physical Review Letters*, 89:257901, 2002.

[15] Mark M. Wilde. *Quantum Information Theory.* Cambridge University Press, 2013.